
Coupling influence of ship dynamic flexure on high accuracy transfer alignment

Wei Wu

School of Opto-Electronic Science and Engineering,
National University of Defense Technology,
Changsha 410073, China
and
Electronics and Computer Science,
University of Southampton,
Southampton SO17 1BJ, UK
E-mail: ww6g11@ecs.soton.ac.uk

Shiqiao Qin

School of Science,
National University of Defense Technology,
Changsha 410073, China
E-mail: sqqin8@nudt.edu.cn

Sheng Chen*

Electronics and Computer Science,
University of Southampton,
Southampton SO17 1BJ, UK
and
Faculty of Engineering,
King Abdulaziz University,
Jeddah 21589, Saudi Arabia
E-mail: sqc@ecs.soton.ac.uk
*Corresponding author

Abstract: This work investigates a new error source for angular velocity or attitude-based transfer alignment, which is caused by the coupling influence of dynamic flexure with ship angular motion. Most traditional studies do not consider this coupling error, as they often assume that dynamic flexure and ship angular motion are uncorrelated. However, the correlation between the dynamic flexure and the ship angular motion generally exists, which will cause a static error in measurements. We adopt the Bernoulli-Euler beam as a simplified ship vibration model to obtain the phase and amplitude relationships for the ship dynamic flexure angle and the ship angular motion. Simulation experiments are then conducted to test the phase delay on alignment accuracy based on the angular velocity matching approach. It is found that the estimation error has a strong correlation with this phase delay, and the error behaves like a sin wave function with the phase delay angle variation. The coupling error of ship dynamic flexure with ship angular velocity is deduced based on the spatial geometric modelling method, and the analysis demonstrates that this coupling error exists in angular velocity or attitude matching systems, which depends on the phase delay and amplitude ratio of ship dynamic flexure and angular velocity.

Keywords: transfer alignment; dynamic flexure; angular velocity matching; phase delay.

Reference to this paper should be made as follows: Wu, W., Qin, S. and Chen, C. (2013) 'Coupling influence of ship dynamic flexure on high accuracy transfer alignment', *Int. J. Modelling, Identification and Control*, Vol. 19, No. 3, pp.224–234.

Biographical notes: Wei Wu is a PhD candidate in School of Opto-Electronic Science and Engineering, National University of Defense Technology, China. He is currently a visiting PhD student with Electronics and Computer Science, University of Southampton. His research interests are in opto-electronic device measurement, control and model identification.

Shiqiao Qin is a Professor in School of Science, National University of Defense Technology, China. He is currently the head of School of Science. His research interests include nano-optics, opto-electronic device measurement, control and optical information processing.

Sheng Chen received his BEng from Huadong Petroleum Institute, China in 1982, and PhD from City University, London, UK in 1986, both in Control Engineering. He was awarded DSc by University of Southampton, UK in 2005. He has been with Electronics and Computer Science, University of Southampton since 1999. He is a Distinguished Adjunct Professor at King Abdulaziz University, Jeddah, Saudi Arabia. He is a fellow of IET and IEEE. His research interests include wireless communications, machine learning, intelligent control systems and evolutionary computation.

1 Introduction

Large ships are often equipped with arrays of peripheral apparatus, such as radar, launching vehicles and optoelectronic sensors, whose attitudes must be determined to a high degree of accuracy when in service. Transfer alignment (TA) is an important approach to align these equipments by using accurate information from the master inertial navigation system (MINS) of the ship (Schnider, 1983). The MINS measures the rotation rates and accelerations along three orthogonal axis to propagate the position, velocity and attitude (Zhang et al., 2012). The difference measured for these three values by the MINS and the slave inertial navigation system (SINS) contains the misalignment angle information of the two coordinate frames, and can be resolved by utilising Kalman filtering methods. TA procedures are mature due to extensive research and have found successful applications to numerous airborne and shipboard systems (Lawrence, 1966; Browne and Lackowski, 1976; Kain and Cloutier, 1989; Spalding, 1992; Groves, 2003; Majeed and Fang, 2009). For shipboard system alignment, angular rate and attitude matching methods are proved to be more feasible than velocity matching methods, because rapid manoeuvre will cause large level-arm estimation error, which will decrease the velocity matching alignment accuracy (Browne and Lackowski, 1976; Majeed and Fang, 2009).

The challenge of angular velocity and attitude matching methods for high accuracy shipboard equipment alignment is how to utilise the physical error model to separate and identify various alignment errors, such as instrument errors and ship dynamic flexure influence. According to the study (Zheng et al., 2011), the gyro error may result in non-linear measurement error, but this error is observable and can be compensated using feedback methods. Another error source is the ship dynamic flexure error, which is caused by the ship motion from waves and manoeuvres and the vibration due to a variety of sources. The works (Day and Arrud, 1999; Petovello et al., 2009) demonstrate that the maximum value of ship dynamic flexure can reach several millirads (mrad), which is unacceptable for high accuracy shipboard devices. To reduce the dynamic flexure influence, extensive works have studied ship dynamic flexure modelling and compensation approaches in the recent years (Mochalov and Kazantsev, 2002; Sun et al., 2007; Joon and Lim, 2009), among which the second-order Markov stochastic process is mostly adopted to depict the dynamic flexure according to its time characteristics.

Most existing studies on TA treat the dynamic flexure and the ship angular motion as two uncorrelated processes

(Sun et al., 2007; Majeed and Fang, 2009; Joon and Lim, 2009). However, from our previous shipboard measurements and laboratory experiments¹, we have found that the TA procedure has a large static estimation error even when the MINS and SINS are all equipped with high-quality gyro instruments and the dynamic flexure model parameters are determined. In other words, an inherent measurement error exists which may be caused by the coupling influence of dynamic flexure and ship angular motion. The works (Browne and Lackowski, 1976; Mochalov, 1999) also mentioned that the alignment error and estimation time has strong correlation with the ship angular motion and ship dynamic flexure. However, no previous analysis was carried out to investigate this issue further. The dynamic flexure and angular motion are all the response of the ship structure to the wave loads (Jensen and Dogliani, 1996; Wu and Sheu, 1996) and, therefore, they are likely to be correlated in general. Thus, a coupling error is introduced by the projection of the additional dynamic flexure velocity on the ship angular velocity. This has important implications. For example, in a high accuracy attitude requirement environment, such as the shipboard missile defense system (Day and Arrud, 1999) which requires about 0.1 mrad alignment accuracy, it is critical to take into account this coupling influence of the ship dynamic flexure and ship angular motion.

This motivates our current study to investigate the alignment error caused by the coupling influence of the dynamic flexure with the ship attitude motion in angular velocity or attitude matching methods. It is worth emphasising that this study is neither about the modelling of dynamic flexure nor about the modelling of ship angular motion. Unlike most of the existing works which assume that the dynamic flexure and the ship angular motion are uncorrelated, our aim is to demonstrate that these two processes are inherently correlated, and our study analyses this correlation relationship. In Section 2, the angular velocity matching function and Kalman filtering model are introduced. Section 3 endeavours to establish a mathematical relationship between the dynamic flexure and the ship angular motion by utilising a simplified ship vibration model, based on which the gyros data for the MINS and SINS are simulated. Following this, the simulation experiments are carried out and the results are analysed in Section 4. Specifically, analysis shows that a phase angle difference exists between the dynamic flexure angle and the ship attitude angle, which will cause a significant estimation error in high accuracy TA. A coupling error function is deduced based on the spatial

geometric modelling and mathematical analysis. The results obtained clear demonstrate that the coupling error depends on the phase delay and amplitude ratio of the dynamic flexure and ship angular velocity. Finally, our conclusions and remarks are presented in Section 5.

2 TA approach

Consider three different coordinates whose coordinate frames are defined respectively as follows

- 1 *Inertial reference coordinate frame (i-frame)*, whose origin is at the centre O_i of the Earth. The x -axis is positive along the Earth's east direction, the y -axis lies in the Earth's north direction, and the z -axis is vertical upward.
- 2 *Ship body coordinate frame (b-frame)*, whose origin is at the centre O_b of the ship. The x -axis is positive along the longitudinal axis of the ship body, the y -axis is perpendicular to the horizontal plane upward, and the z -axis complements the right-hand rule.
- 3 *Peripheral sensor body frame (s-frame)*, whose origin is at the centre O_s of the perpendicular sensor centre, and the coordinates are accordance with the sensor measurement frame coordinates.

2.1 Angular velocity matching function

As shown in Figure 1, assume that the MINS's coordinates $O_m(x_m, y_m, z_m)$ have been aligned with the b -frame, and the SINS's coordinates $O_s(x_s, y_s, z_s)$ are in accordance with the s -frame. When serviced in the sea, the ship will undergo angular rotation with respect to the inertial space, caused by wave or wind induced pitching, rolling and yawing, as well as purposeful turning manoeuvres. If the ship hull is rigid, the angular velocities measured by the MINS and SINS with respect to the i -frame are equal. Since the ship hull is elastic, the bending will cause an additional angular rotation for the SINS, relative to the MINS. When this flexure changes in time, there is an additional angular velocity measured by the SINS but not by the MINS. In Figure 1, φ is the total misalignment Euler angle between the MINS and SINS, which includes a static component ϕ_0 and a dynamic component θ . Provided that the misalignment angle can be compensated to within several mrad using the initial course estimation results, in other words, if the misalignment angle is small, the relationship between φ , ϕ_0 and θ can be written in a vector form

$$\varphi = \phi_0 + \theta. \quad (1)$$

The detailed derivation of equation (1) is given in the Appendix.

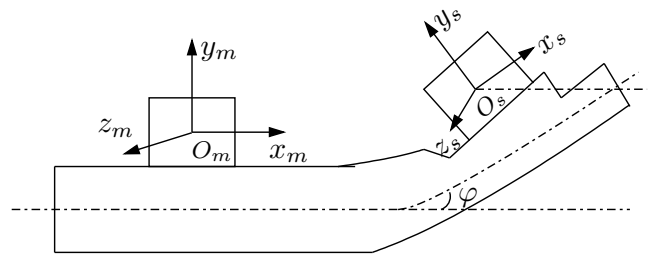
The MINS measures the ship inertial angular velocity projected onto the $O_m(x_m, y_m, z_m)$ coordinates, which can be written as $\vec{\Omega}_{ib}^b$, while the SINS measures

the ship inertial angular velocity projected onto the $O_s(x_s, y_s, z_s)$ coordinates, denoted as $\vec{\Omega}_{ib}^s$. The angular velocity relationship can be expressed as (Mochalov and Kazantasev, 2002)

$$\vec{\Omega}_{ib}^s = C_b^s(\varphi)\vec{\Omega}_{ib}^b + \dot{\theta}, \quad (2)$$

where $C_b^s(\varphi)$ denotes the direction cosine matrix (DCM) from the b -frame to the s -frame, and $\dot{\theta}$ an additional velocity caused by the dynamic flexure of the s -frame relative to the b -frame, while the dot operator ($\dot{\bullet}$) represents the differentiation with respect to time t . The expression of a DCM can be found in the Appendix.

Figure 1 Schematic diagram of ship angular measurement



The difference between the angular velocities measured by the MINS and SINS with respect to the b -frame is therefore given by

$$\Delta\vec{\Omega} = \vec{\Omega}_{ib}^b - \vec{\Omega}_{ib}^s = [\mathbf{I}_3 - C_b^s(\varphi)]\vec{\Omega}_{ib}^b - \dot{\theta}, \quad (3)$$

where \mathbf{I}_3 denotes the 3×3 identity matrix. If the misalignment angle is small, that is, the misalignment angle can be compensated to within several mrad by the initial course alignment, equation (3) can be approximated as (Mochalov and Kazantasev, 2002)

$$\Delta\vec{\Omega} \approx \hat{\Omega}_{ib}^b \varphi - \dot{\theta}, \quad (4)$$

where $\hat{\Omega}_{ib}^b$ is a skew-symmetric matrix with the form

$$\hat{\Omega}_{ib}^b = \begin{bmatrix} 0 & \Omega_{ibz}^b & -\Omega_{iby}^b \\ -\Omega_{ibz}^b & 0 & \Omega_{ibx}^b \\ \Omega_{iby}^b & -\Omega_{ibx}^b & 0 \end{bmatrix}, \quad (5)$$

while $(\Omega_{ibx}^b, \Omega_{iby}^b, \Omega_{ibz}^b)$ are the three coordinate values of $\vec{\Omega}_{ib}^b$. As can be seen from equations (4) and (5), the rank of $\hat{\Omega}_{ib}^b$ is $r = 2$, while the dimension of the vectors involved is $n = 3$. Since $r < n$, the differential equation (4) has no analytical solution. One approach to determine the misalignment angle is to take successive measurements and to apply a Kalman filter.

2.2 Kalman filtering function

For processing with a Kalman filter, the measurement function for equation (4) is presented in a standard matrix form as

$$z = \mathbf{H}\mathbf{x} + \mathbf{v}, \quad (6)$$

where z and v are the 3×1 measurement vector and measurement error vector, respectively, while H and x denote the measurement matrix and the state vector, respectively.

Assume that the MINS and SINS are all the ring laser gyro (RLG) systems, and the instrument noise includes the gyro constant bias $\bar{\varepsilon}$ and the gyro random walk noise $\tilde{\varepsilon}$. Then the state vector is of the size 15×1 , specified by

$$x = [\phi_{0x} \ \phi_{0y} \ \phi_{0z} \ \theta_x \ \theta_y \ \theta_z \ \dot{\theta}_x \ \dot{\theta}_y \ \dot{\theta}_z \ \Delta\bar{\varepsilon}_x \ \Delta\bar{\varepsilon}_y \ \Delta\bar{\varepsilon}_z \ \Delta\tilde{\varepsilon}_x \ \Delta\tilde{\varepsilon}_y \ \Delta\tilde{\varepsilon}_z]^\top, \quad (7)$$

where $^\top$ denotes the vector and matrix transpose operator, $(\phi_{0x}, \phi_{0y}, \phi_{0z})$, $(\theta_x, \theta_y, \theta_z)$ and $(\dot{\theta}_x, \dot{\theta}_y, \dot{\theta}_z)$ are the three coordinate values of ϕ_0 , θ and $\dot{\theta}$, respectively, while $(\Delta\bar{\varepsilon}_x, \Delta\bar{\varepsilon}_y, \Delta\bar{\varepsilon}_z)$ and $(\Delta\tilde{\varepsilon}_x, \Delta\tilde{\varepsilon}_y, \Delta\tilde{\varepsilon}_z)$ are the three coordinate values of the gyro constant bias difference $\Delta\bar{\varepsilon}$ and the gyro random walk noise difference $\Delta\tilde{\varepsilon}$ between the MINS and SINS, respectively. The 3×15 measurement matrix is given by

$$H = \begin{bmatrix} \hat{\Omega}_{ib}^b & \hat{\Omega}_{ib}^b & -I_3 & I_3 & I_3 \end{bmatrix}. \quad (8)$$

In various applications (Browne and Lackowski, 1976; Schnider, 1983; Mochalov and Kazantsev, 2002; Majeed and Fang, 2009), the dynamic flexure is typically modelled by three independent second-order Markov processes for pitching, rolling and yawing, respectively. The related differential equation can be written as (Mochalov and Kazantsev, 2002)

$$\ddot{\theta}_i + 2\mu_i\dot{\theta}_i + b_i^2\theta_i = 2b_i\sigma_i\sqrt{\mu_i}e_i(t), \quad (9)$$

where the index i indicates the x , y or z coordinate, μ_i is the irregularity coefficient, b_i is the prevailing variation frequency and σ_i is the standard deviation of the dynamic flexure, while $e_i(t)$ is a Gaussian white noise with unit variance. The gyro random walk noise on the other hand can be represented using three independent first-order Markov processes (Schnider, 1983)

$$\dot{\tilde{\varepsilon}}_i + \tilde{\mu}_i\tilde{\varepsilon}_i = \tilde{\sigma}_i\sqrt{2\tilde{\mu}_i}\tilde{e}_i(t), \quad (10)$$

where $\tilde{\mu}_i$ is the irregularity coefficient, $\tilde{\sigma}_i$ is the standard deviation of the gyro random walk noise, and $\tilde{e}_i(t)$ is a Gaussian white noise with unit variance.

Remark 1: The dynamic flexure is induced by wave or wind induced load on the ship structure, which is traditionally modelled as a second-order Markov process (Browne and Lackowski, 1976). Most of the works choose three independent second-order Markov processes to model the dynamic flexure on the pitch, roll and yaw axes, respectively. We also adopt this approach to simplify the analysis. Researchers are well aware that more accurate dynamic flexure model, possibly involving the three components of the dynamic flexure being correlated, may be desirable in applications, depending on the accuracy requirement (Schnider, 1983). Actually, we may also point out that the true dynamic flexure may exhibit non-linear

dynamics and, therefore, accurate modelling would involve non-linear dynamic model. However, the focus of our study is on investigating the coupling influence of the dynamic flexure with the ship angular motion, not on accurate modelling of dynamic flexure. The simplified model (9) is sufficient for our purpose. In fact, if we can demonstrate that the dynamic flexure and the ship angular motion are correlated under this simplified dynamic flexure model, then the true dynamic flexure process, whose three components are not independent, will surely be correlated with the ship angular motion.

The state equation for the Kalman filter is then defined as

$$\dot{x} = Fx + w, \quad (11)$$

where the state-space equation matrix F takes the form

$$F = \begin{bmatrix} O_{3 \times 3} & O_{3 \times 6} & O_{3 \times 6} \\ O_{6 \times 3} & F_{6 \times 6}^1 & O_{6 \times 6} \\ O_{6 \times 3} & O_{6 \times 6} & F_{6 \times 6}^2 \end{bmatrix}, \quad (12)$$

with $O_{l \times m}$ denoting the $l \times m$ zero matrix, and

$$F_{6 \times 6}^1 = \begin{bmatrix} O_{3 \times 3} & I_3 \\ -b_x^2 & 0 & 0 & -2\mu_x & 0 & 0 \\ 0 & -b_y^2 & 0 & 0 & -2\mu_y & 0 \\ 0 & 0 & -b_z^2 & 0 & 0 & -2\mu_z \end{bmatrix}, \quad (13)$$

$$F_{6 \times 6}^2 = \begin{bmatrix} O_{3 \times 3} & O_{3 \times 3} \\ -\tilde{\mu}_x & 0 & 0 & O_{3 \times 3} \\ 0 & -\tilde{\mu}_y & 0 & O_{3 \times 3} \\ 0 & 0 & -\tilde{\mu}_z & O_{3 \times 3} \end{bmatrix}. \quad (14)$$

The 15×1 state noise vector w has the covariance matrix

$$E[ww^\top] = \text{diag} \left\{ \underbrace{0, \dots, 0}_6, 4b_x^2\sigma_x^2\mu_x, 4b_y^2\sigma_y^2\mu_y, 4b_z^2\sigma_z^2\mu_z, 0, 0, 0, 2\tilde{\mu}_x\tilde{\sigma}_x^2, 2\tilde{\mu}_y\tilde{\sigma}_y^2, 2\tilde{\mu}_z\tilde{\sigma}_z^2 \right\}, \quad (15)$$

where $E[\bullet]$ denotes the expectation operator.

In the procedure of measurement, the Kalman filter acts as an observer, and the misalignment angle between the MINS and SINS frames can be optimally estimated by utilising the dynamic flexure model.

3 Angular motion and dynamic flexure modelling

According to the hydrodynamic principle, ship angular motion and dynamic flexure are all the responses of ship to sea wave loadings (Jensen and Dogliani, 1996; Gu et al., 2011). In theoretical and numerical analysis, the Bernoulli-Euler beam is usually adopted to depict a simplified ship hull model (Wu and Sheu, 1996; Watanabe and Soares, 1999; Abu-Hilal and Mohsen, 2000). In order to study the coupling error influence, the phase and amplitude relationships for dynamic flexure angle and ship attitude angle are deduced based on the Bernoulli-Euler beam function. Then, the simulation data is generated using this relationship.

3.1 Attitude and dynamic flexure model

The transverse vibration of a uniform elastic Euler-Bernoulli beam is described by the partial differential equation (Abu-Hilal and Mohsen, 2000)

$$EI \frac{\partial^4 y}{\partial x^4} + m\ddot{y} + \beta\dot{y} = q(x, t), \tag{16}$$

where EI is the flexure rigidity of the beam, m is the mass per unit length of the beam, β is the damping coefficient, and $q(x, t)$ is the excitation force.

When $q(x, t) = 0$, the solution for the free vibration function is defined as

$$y(x, t) = \sum_{k=1}^{\infty} X_k(x)p_k(t), \tag{17}$$

where $y(x, t)$ denotes the total linear displacement which includes the rigid motion displacement $y_r(x, t)$ and the elastic motion displacement $y_d(x, t)$, k denotes the k^{th} mode of the beam, $p_k(t)$ is the k^{th} generalised deflection mode of the beam, and $X_k(x)$ is the k^{th} normal mode of the beam which takes the form

$$X_k(x) = A_k \sin(G_k x) + B_k \cos(G_k x) + C_k \sinh(G_k x) + D_k \cosh(G_k x). \tag{18}$$

In equation (18), A_k, B_k, C_k, D_k and G_k are constants that are determined by the boundary conditions of the beam. Considering the ship hull floating on the waves, the free boundary conditions at the two ends can be given as

$$\begin{cases} \frac{\partial^2 X_k(x)}{\partial x^2} \Big|_{x=0} = 0, & \frac{\partial^3 X_k(x)}{\partial x^3} \Big|_{x=0} = 0, \\ \frac{\partial^2 X_k(x)}{\partial x^2} \Big|_{x=l} = 0, & \frac{\partial^3 X_k(x)}{\partial x^3} \Big|_{x=l} = 0, \end{cases} \tag{19}$$

where l is the length of the beam. Substituting equation (19) into equation (18) yields the matrix equation

$$\begin{bmatrix} 0 & -1 & 0 & 1 \\ -1 & 0 & 1 & 0 \\ -\sin(G_k l) - \cos(G_k l) \sinh(G_k l) \cosh(G_k l) \\ -\cos(G_k l) \sin(G_k l) \cosh(G_k l) \sinh(G_k l) \end{bmatrix} \begin{bmatrix} A_k \\ B_k \\ C_k \\ D_k \end{bmatrix} = 0. \tag{20}$$

The condition for equation (20) to have a unique solution requires that the determinant of the 4×4 matrix equals to zero, which leads to

$$\cos(G_k l) \cosh(G_k l) = 1. \tag{21}$$

Notice that equation (21) is a transcendental equation with the roots

$$\begin{cases} G_1 l = 0, \\ G_2 l = 4.73, \\ G_3 l = 7.85, \\ \vdots \end{cases} \tag{22}$$

When $q(x, t) \neq 0$, we substitute equation (17) into equation (16) and multiply the both sides of the equation by

$X_j(x)$. Then, integrating the resulting equation with respect to x between 0 and l yields

$$\begin{aligned} & \sum_{k=1}^{\infty} \int_0^l \left(EI \frac{\partial^4 X_k}{\partial x^4} X_j p_k + m \ddot{p}_k X_k X_j + \beta \dot{p}_k X_k X_j \right) dx \\ & = \int_0^l X_j q(x, t) dx. \end{aligned} \tag{23}$$

By considering the orthogonality condition

$$\int_0^l X_k X_j dx = \int_0^l \frac{\partial^4 X_k}{\partial x^4} X_j dx = 0, \text{ for } k \neq j, \tag{24}$$

we derive the differential equation of the k^{th} generalised deflection mode as

$$\ddot{p}_k(t) + 2\omega_k \xi_k \dot{p}_k(t) + \omega_k^2 p_k(t) = Q_k(t), \tag{25}$$

where the k^{th} natural circular frequency ω_k , damping ratio ξ_k and generalised force Q_k are expressed respectively as follows

$$\omega_k = \sqrt{\frac{G_k}{M_k}} = K_k^2 \sqrt{\frac{EI}{m}}, \tag{26}$$

$$\xi_k = \frac{\beta}{2\sqrt{K_k M_k}}, \tag{27}$$

$$Q_k(t) = \frac{1}{M_k} \int_0^l X_k(x) q(x, t) dx, \tag{28}$$

with the generalised stiffness K_k and generalised mass M_k for the k^{th} mode given by

$$K_k = \int_0^l EI \frac{\partial^4 X_k}{\partial x^4} X_k dx, \tag{29}$$

$$M_k = \int_0^l m X_k^2(x) dx. \tag{30}$$

Assume that the excitation force distribution along the beam is

$$q(x, t) = F_0 \sin(\omega t), \tag{31}$$

where ω is the circular frequency of the excitation force and F_0 is the constant force amplitude. Substituting equation (31) into equation (25), we obtain the steady-state solution

$$p_k(t) = c_k \sin(\omega t + \psi_k), \tag{32}$$

where the k^{th} response amplitude c_k is given by

$$c_k = \frac{F_0 \lambda_k^2}{M_k \omega^2 \sqrt{(1 - \lambda_k^2)^2 + (2\xi_k \lambda_k)^2}} \int_0^l X_k(x) dx, \tag{33}$$

and the k^{th} phase delay angle ψ_k is defined by

$$\psi_k = \arctan \frac{2\xi_k \lambda_k}{\lambda_k^2 - 1}, \tag{34}$$

in which $\lambda_k = \omega/\omega_k$ denotes the frequency ratio.

According to equation (22), we can see $G_1 = 0$, while from equation (26) we can obtain $\omega_1 = 0$. Then, it can be shown that the first order normal mode is given as

$$X_1(x) = ax + b, \quad (35)$$

where a and b are the constants determined by the initial displacement conditions of the beam according to

$$\begin{cases} a = \frac{\partial y(x,t)}{\partial x} \Big|_{x=l} - \frac{\partial y(x,t)}{\partial x} \Big|_{x=0}, \\ b = y(l,t) - y(0,t). \end{cases} \quad (36)$$

On the other hand, the first generalised deflection mode is given by

$$p_1(t) = c_1 \sin(\omega t), \quad (37)$$

with

$$c_1 = \frac{3F_0(al + 2b)}{2m\omega^2(a^2l^2 + 3abl + 3b^2)}. \quad (38)$$

As a result, the rigid body displacement $y_r(x,t)$ can be written as

$$y_r(x,t) = X_1(x)p_1(t) = c_1(ax + b) \sin(\omega t). \quad (39)$$

The rigid body rotation angle around the z -axis can then be derived by

$$\Theta_z(t) = \frac{\partial y_r(x,t)}{\partial x} = c_1 a \sin(\omega t). \quad (40)$$

For $k > 1$, the natural circular frequency $\omega_k \neq 0$. The elastic motion displacement $y_d(x,t)$ can be derived by

$$y_d(x,t) = \sum_{k=2}^{\infty} X_k(x)c_k \sin(\omega t + \psi_k). \quad (41)$$

Thus, the dynamic flexure angle around the z -axis is approximated by

$$\theta_z(x,t) = \frac{\partial y_d(x,t)}{\partial x} = \sum_{k=2}^{\infty} \frac{\partial X_k(x)}{\partial x} c_k \sin(\omega t + \psi_k). \quad (42)$$

The amplitude ratio of the ship attitude and dynamic flexure can be defined as

$$T_z(x) = \frac{c_1 a}{\sum_{k=2}^{\infty} \frac{\partial X_k(x)}{\partial x} c_k}. \quad (43)$$

For simplicity and tractability reasons, if we assume that the ship attitude motion and dynamic flexure are rotational symmetry, then the relationships for rolling and yawing can be approximated in the same way.

3.2 Attitude and dynamic flexure data generation

Compared equation (40) with equation (42), it can be seen that the attitude motion and the dynamic flexure angle have the same angular frequency of the excited force frequency. In an analysis of aircraft vibration using the exactly same Bernoulli-Euler beam driven by white noise, Lee and Whaley (1976) have shown that the second-order

vibration mode contributes about 93% of the total energy in the dynamic flexure. It is reasonable to believe that in our case the second-order vibration mode will account for the majority of the total energy in the dynamic flexure. Therefore, we will also approximate the dynamic flexure by the second-order vibration mode. More specifically, we approximate the dynamic flexure angle θ_z by

$$\theta_z \approx \frac{\partial X_2(x)}{\partial x} c_2 \sin(\omega t + \psi_2) = \frac{\partial X_2(x)}{\partial x} c_2 \sin(\omega t + \psi_z),$$

while approximating the amplitude ratio T_z by

$$T_z \approx \frac{c_1 a}{\frac{\partial X_2(x)}{\partial x} c_2}.$$

Applying the same approximation to the relationships for rolling and yawing, we obtain the phase delay Euler angles, (ψ_x, ψ_y, ψ_z) , around the x , y and z axes, respectively, as well as the amplitude ratio matrix \mathbf{T}

$$\mathbf{T} = \begin{bmatrix} T_x & 0 & 0 \\ 0 & T_y & 0 \\ 0 & 0 & T_z \end{bmatrix}. \quad (44)$$

We will also refer to $(\Theta_x, \Theta_y, \Theta_z)$ as the attitude Euler angles around the x , y and z axis, respectively.

The ship attitude angle can be derived by rotating the given dynamic flexure by an angle ψ and multiplying the result with the amplitude ratio \mathbf{T}

$$\begin{bmatrix} \Theta_x \\ \Theta_y \\ \Theta_z \end{bmatrix} = \mathbf{T} \mathbf{C}(\psi) \begin{bmatrix} \theta_x \\ \theta_y \\ \theta_z \end{bmatrix}, \quad (45)$$

in which the DCM $\mathbf{C}(\psi)$ can be approximately calculated by

$$\mathbf{C}(\psi) = \begin{bmatrix} 1 & -\psi_z & \psi_y \\ \psi_z & 1 & -\psi_x \\ -\psi_y & \psi_x & 1 \end{bmatrix}, \quad (46)$$

if the rotation angle ψ is small, as explained in the Appendix.

Table 1 Model parameters of dynamic flexure

	μ_i (rad/s ²)	b_i (rad/s)	σ_i (mrad)
Pitching angle	0.013	1.010	0.282
Rolling angle	0.006	1.414	0.490
Yawing angle	0.024	1.180	0.380

In our simulation, the dynamic flexure angles are treated as three independent second-order Markov processes whose parameters are identified from the real measurement data. The identified parameters μ_i , b_i and σ_i for equation (9) are listed in Table 1, while Figure 2 shows the pitching angle of the dynamic flexure generated by using the given parameters.

The attitude Euler angles of the MINS, denoted as Θ^{MINS} , are then derived based on the generated dynamic flexure angles according to equation (45). Figure 3 depicts the pitching angle curve so generated

at the condition of $\psi = [5 \text{ deg } 5 \text{ deg } 5 \text{ deg}]^T$ and $T_x = T_y = T_z = 300$. Assume that the course alignment between the MINS and SINS has been completed and the static misalignment angles between the MINS and SINS are $\phi_0 = [0.2 \text{ deg } 0.2 \text{ deg } 0.2 \text{ deg}]^T$. Then the attitude Euler angles of the SINS, denoted as Θ^{SINS} , can be obtained by rotating Θ^{MINS} with the angle φ , where φ is defined in equation (1). More specifically, $\Theta^{\text{SINS}} = C(\varphi)\Theta^{\text{MINS}}$, with $C(\varphi)$ taking the same form of equation (46) by substituting ψ with φ .

Figure 2 Pitching dynamic flexure angle (see online version for colours)

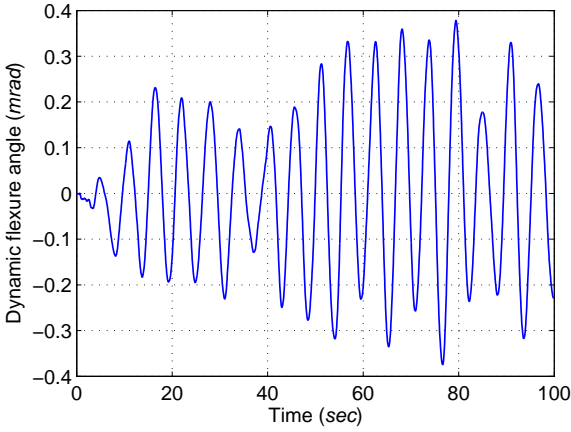
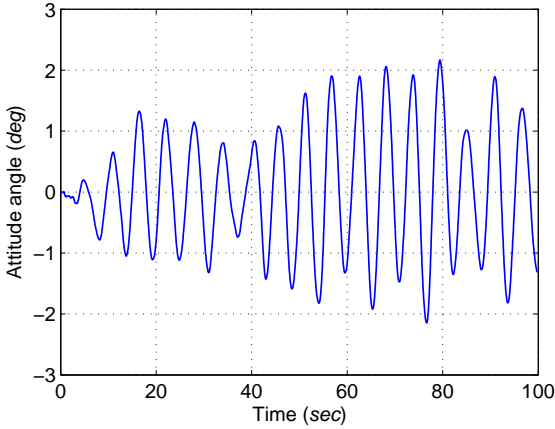


Figure 3 Pitching attitude angle (see online version for colours)



To obtain the gyro output sample values of the MINS and SINS for the test, the gyro noise parameters are given as follows:

- 1 The constant biases of the MINS gyros are $\bar{\epsilon}_{\text{MINS}} = [0.005 \text{ deg/hr } 0.005 \text{ deg/hr } 0.005 \text{ deg/hr}]^T$, and the related random walk noises are $\tilde{\epsilon}_{\text{MINS}} = [0.001 \text{ deg}/\sqrt{\text{hr}} \ 0.001 \text{ deg}/\sqrt{\text{hr}} \ 0.001 \text{ deg}/\sqrt{\text{hr}}]^T$;
- 2 The constant biases of the SINS gyros are $\bar{\epsilon}_{\text{SINS}} = [0.02 \text{ deg/hr } 0.02 \text{ deg/hr } 0.02 \text{ deg/hr}]^T$, and the related random walk noises are $\tilde{\epsilon}_{\text{SINS}} = [0.005, \text{ deg}/\sqrt{\text{hr}} \ 0.005 \text{ deg}/\sqrt{\text{hr}} \ 0.005 \text{ deg}/\sqrt{\text{hr}}]^T$.

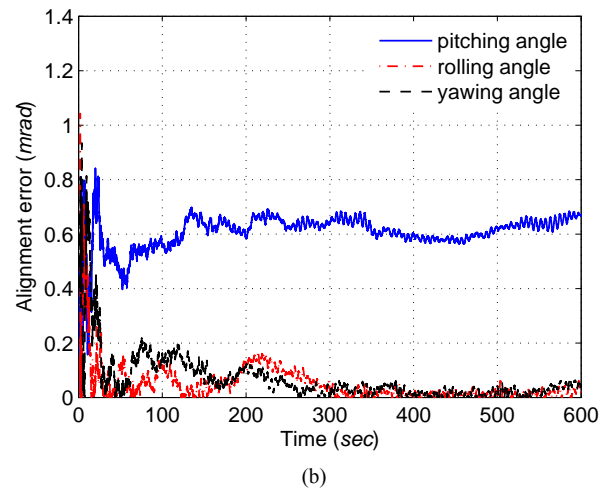
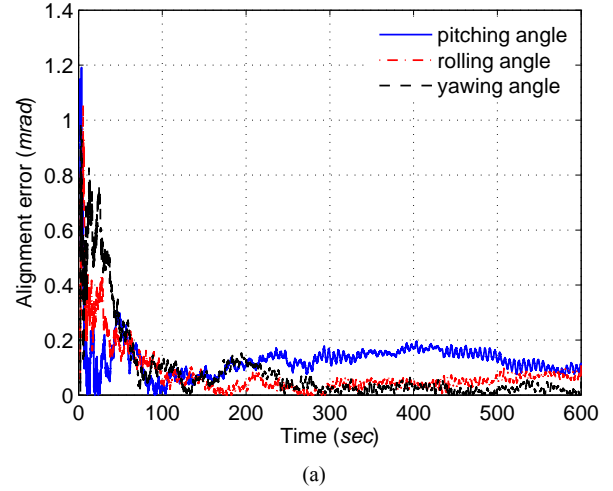
The generated gyro data of the MINS and SINS contain the phase and amplitude relationship between the ship attitude and the dynamic flexure, which will be processed by using the Kalman filtering method.

4 Simulation results and analysis

4.1 Simulation results

We first fixed the amplitude ratios for the dynamic flexure and ship attitude to $T_x = T_y = T_z = 300$, and performed a number of simulation runs to investigate the alignment performance under different phase delay angles. When there existed no phase delay, i.e., $\psi = \mathbf{0}$, the alignment results obtained are shown in Figure 4(a), where it can be seen that the alignment errors for the three coordinates are all within 0.1 mrad at the end of 10-minutes alignment. For the case of $\psi_z = 5 \text{ deg}$ and $\psi_x = \psi_y = 0$, the alignment error of the pitching angle reaches the value of 0.65 mrad, as can be seen in Figure 4(b).

Figure 4 Alignment errors for different phase delay angles given $T_x = T_y = T_z = 300$, (a) no phase delay and (b) $\psi_x = \psi_y = 0$ and $\psi_z = 5 \text{ deg}$ (see online version for colours)



When the phase delay angles of the (x, y, z) coordinates increased simultaneously from 0 to π by 5 deg increment, the alignment errors obtained at the end of ten minutes alignment are shown in Figure 5. It can be observed that the estimation error varied dramatically as the phase delay angle increased. The minimum errors were found around the angles of 0, $\frac{\pi}{2}$ and π , while the maximum values were reached around the angles of $\frac{\pi}{4}$ and $\frac{3\pi}{4}$. Specifically, the coupling error of dynamic flexure and ship attitude behaves like a sin function as the phase delay angle increases, given the fixed $T_x = T_y = T_z = 300$, and the maximum alignment errors can reach to 5.0 mrad, 6.1 mrad and 6.4 mrad for the pitching, rolling and yawing angles, respectively.

Figure 5 Alignment error as the function of the phase delay angle $\psi_x = \psi_y = \psi_z$ varying from 0 to π , given $T_x = T_y = T_z = 300$ (see online version for colours)

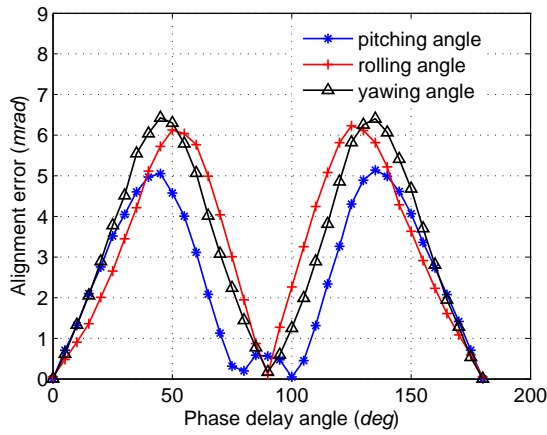
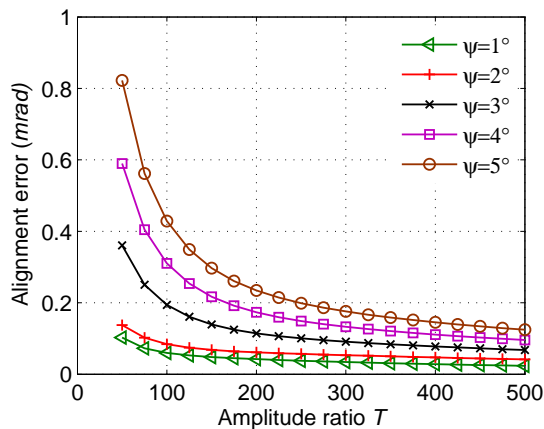


Figure 6 Alignment error as the function of the amplitude ratio $T_x = T_y = T_z = T$ for different phase delay angle values $\psi_x = \psi_y = \psi_z = \psi$ (see online version for colours)



Next, we set $T_x = T_y = T_z = T$ and further investigated the influence of the amplitude ratio value T to the alignment accuracy. Given different values of the phase delay angle, $\psi_x = \psi_y = \psi_z = \psi$, Figure 6 depicts the corresponding alignment error curves as the function of the amplitude ratio $T_x = T_y = T_z = T$. The simulation results

show that both the amplitude ratio and the phase delay angle have significant influence to the alignment accuracy. Specifically, the smaller the amplitude ratio T , the larger the alignment error, while the alignment error decreases as the phase delay angle ψ decreases.

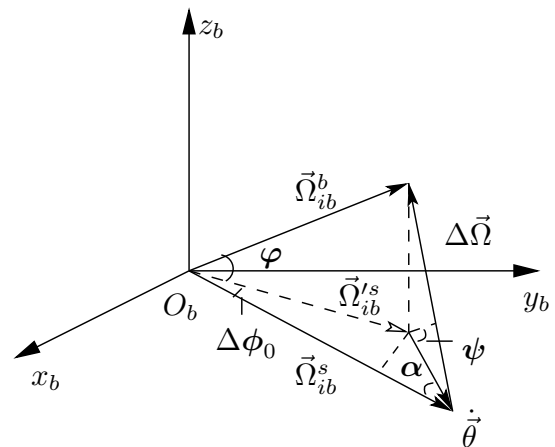
From the above simulation results, it can be observed that the standard TA procedure, as outlined in Section 2, results in an inherent estimation error, which agrees with our previous shipboard measurement and laboratory experiment data. The results also show that this estimation error is correlated with the phase delay angle between the dynamic flexure and the ship angular motion. However, this coupling error has not been drawn sufficient attention in the previous literatures which often treat the dynamic flexure and the ship angular motion as two independent processes in theoretical study and simulation test (Sun et al., 2007; Majeed and Fang, 2009; Joon and Lim, 2009). This is the underlying cause of the significant alignment error of the standard TA procedure. Below, we present an analysis of this coupling error.

4.2 Coupling error modelling

A simple approach to derive this coupling error function is to use a geometric modelling method. According to equation (4), the angular velocity vectors $\vec{\Omega}_{ib}^b$, $\vec{\Omega}_{ib}^s$ and $\vec{\theta}$ are all projected onto the b -frame, and their spatial relationships are illustrated in Figure 7. Thus, the rotation of angular velocity vectors can be explained as follows. Firstly, the MINS angular velocity vector $\vec{\Omega}_{ib}^b$ is rotated by an angle of φ to obtain $\vec{\Omega}_{ib}^s$, and this rotation function can be expressed as

$$\vec{\Omega}_{ib}^s = C_b^s(\varphi)\vec{\Omega}_{ib}^b. \quad (47)$$

Figure 7 Spatial relationship of the angular velocity vectors and the additional dynamic flexure velocity vector



As $|C_b^s(\varphi)| = 1$, the magnitude relationship between $\vec{\Omega}_{ib}^b$ and $\vec{\Omega}_{ib}^s$ is $|\vec{\Omega}_{ib}^b| = |\vec{\Omega}_{ib}^s|$. Considering the additional dynamic flexure velocity $\vec{\theta}$, we obtain the SINS angular velocity vector $\vec{\Omega}_{ib}^s$ given by

$$\vec{\Omega}_{ib}^s = \vec{\Omega}_{ib}^s + \vec{\theta}. \quad (48)$$

If the vector $\vec{\theta}$ is parallel with $\vec{\Omega}_{ib}^s$, the angle between $\vec{\Omega}_{ib}^b$ and $\vec{\Omega}_{ib}^s$ is φ , and the angular velocity matching function is given in equation (4). Otherwise, the additional dynamic flexure velocity $\dot{\vec{\theta}}$ will introduce an coupling error angle $\Delta\phi_0$ and, if $\Delta\phi_0$ is small, the angular velocity matching function can be modified as

$$\begin{aligned}\Delta\vec{\Omega} &= \vec{\Omega}_{ib}^b - \vec{\Omega}_{ib}^s = \vec{\Omega}_{ib}^b - \mathbf{C}_b^s(\varphi + \Delta\phi_0)\vec{\Omega}_{ib}^b - \dot{\vec{\theta}} \\ &\approx \hat{\Omega}_{ib}^b(\varphi + \Delta\phi_0) - \dot{\vec{\theta}},\end{aligned}\quad (49)$$

where $\dot{\vec{\theta}}$ is the projection of $\vec{\theta}$ onto $\vec{\Omega}_{ib}^s$, and its direction is in accordance with $\vec{\Omega}_{ib}^s$. Therefore, $\dot{\vec{\theta}}$ can be expressed as

$$\dot{\vec{\theta}} = \mathbf{M}(\dot{\vec{\theta}})\mathbf{C}(\alpha)\vec{v}_{ib}^s, \quad (50)$$

where α is the angle between the vectors $\vec{\theta}$ and $\vec{\Omega}_{ib}^s$, while the magnitude matrix $\mathbf{M}(\dot{\vec{\theta}})$, the unit direction vector \vec{v}_{ib}^s and the DCM $\mathbf{C}(\alpha)$ are expressed respectively as

$$\mathbf{M}(\dot{\vec{\theta}}) = \begin{bmatrix} |\dot{\theta}_x| & 0 & 0 \\ 0 & |\dot{\theta}_y| & 0 \\ 0 & 0 & |\dot{\theta}_z| \end{bmatrix}, \quad (51)$$

$$\vec{v}_{ib}^s = \frac{\vec{\Omega}_{ib}^s}{|\vec{\Omega}_{ib}^s|}, \quad (52)$$

$$\begin{aligned}\mathbf{C}(\alpha) &= \left(\mathbf{I}_3 - \frac{1}{2}(\hat{\mathbf{S}}_\varphi + \hat{\mathbf{S}}_{\Delta\phi_0})\right)\left(\mathbf{I}_3 - \frac{1}{2}\hat{\mathbf{S}}_\psi\right) \\ &\approx \mathbf{I}_3 - \frac{1}{2}(\hat{\mathbf{S}}_\varphi + \hat{\mathbf{S}}_{\Delta\phi_0} + \hat{\mathbf{S}}_\psi),\end{aligned}\quad (53)$$

in which $\hat{\mathbf{S}}_\varphi$, $\hat{\mathbf{S}}_{\Delta\phi_0}$ and $\hat{\mathbf{S}}_\psi$ are the skew-symmetric matrices of φ , $\Delta\phi_0$ and ψ , respectively, defined similarly to equation (5). Substituting equation (50) into equation (49) yields

$$\begin{aligned}\Delta\vec{\Omega} &\approx \hat{\Omega}_{ib}^b(\varphi + \Delta\phi_0) - \mathbf{M}(\dot{\vec{\theta}})\vec{v}_{ib}^s \\ &\quad + \frac{1}{2}\mathbf{M}(\dot{\vec{\theta}})(\hat{\mathbf{S}}_\varphi + \hat{\mathbf{S}}_{\Delta\phi_0} + \hat{\mathbf{S}}_\psi)\vec{v}_{ib}^s \\ &= \hat{\Omega}_{ib}^b\varphi - \mathbf{M}(\dot{\vec{\theta}})\vec{v}_{ib}^s + \hat{\Omega}_{ib}^b\Delta\phi_0 \\ &\quad - \frac{1}{2}\mathbf{M}(\dot{\vec{\theta}})\hat{\mathbf{S}}_{\vec{v}_{ib}^s}(\varphi + \Delta\phi_0 + \psi) \\ &= \Delta\vec{\Omega}_1 + \Delta\vec{\Omega}_2,\end{aligned}\quad (54)$$

where $\hat{\mathbf{S}}_{\vec{v}_{ib}^s}$ is the skew-symmetric matrix of \vec{v}_{ib}^s , while $\Delta\vec{\Omega}_1$ and $\Delta\vec{\Omega}_2$ are given respectively by

$$\Delta\vec{\Omega}_1 = \hat{\Omega}_{ib}^b\varphi - \mathbf{M}(\dot{\vec{\theta}})\vec{v}_{ib}^s, \quad (55)$$

$$\Delta\vec{\Omega}_2 = \hat{\Omega}_{ib}^b\Delta\phi_0 - \frac{1}{2}\mathbf{M}(\dot{\vec{\theta}})\hat{\mathbf{S}}_{\vec{v}_{ib}^s}(\varphi + \Delta\phi_0 + \psi). \quad (56)$$

From equation (54) which is the correct angular velocity matching function, it becomes clear where the alignment error source comes from in the traditional TA procedure.

Basically, it only takes into account $\Delta\vec{\Omega}_1$ [see equation (4)] and ignores the component $\Delta\vec{\Omega}_2$ or equivalently assumes $\Delta\vec{\Omega}_2 = 0$. However, in doing so it introduces a coupling error $\Delta\phi_0$. This alignment error source may be derived approximately as follows.

Setting $\Delta\vec{\Omega}_2 = 0$ in equation (56) results in

$$\left(\hat{\Omega}_{ib}^b - \frac{1}{2}\mathbf{M}(\dot{\vec{\theta}})\hat{\mathbf{S}}_{\vec{v}_{ib}^s}\right)\Delta\phi_0 = \frac{1}{2}\mathbf{M}(\dot{\vec{\theta}})\hat{\mathbf{S}}_{\vec{v}_{ib}^s}(\varphi + \psi). \quad (57)$$

Differentiating equation (45) with respect to time t results in

$$\vec{\Omega}_{ib}^b = \mathbf{T}\mathbf{C}(\psi)\dot{\vec{\theta}} \quad (58)$$

from which $\dot{\vec{\theta}}$ can be derived as

$$\dot{\vec{\theta}} = \mathbf{C}^T(\psi)\mathbf{T}^{-1}\vec{\Omega}_{ib}^b. \quad (59)$$

Assuming $T_x = T_y = T_z = T$, the magnitude of $\dot{\vec{\theta}}$ is then given by

$$|\dot{\vec{\theta}}| = \frac{1}{T} \left| (\mathbf{I}_3 - \hat{\mathbf{S}}_\psi)\vec{\Omega}_{ib}^b \right|. \quad (60)$$

By substituting the results of equations (58) to (60) into equation (57), the coupling error can be approximated as

$$\Delta\phi_0 \approx \frac{1}{2T}(\varphi + \psi). \quad (61)$$

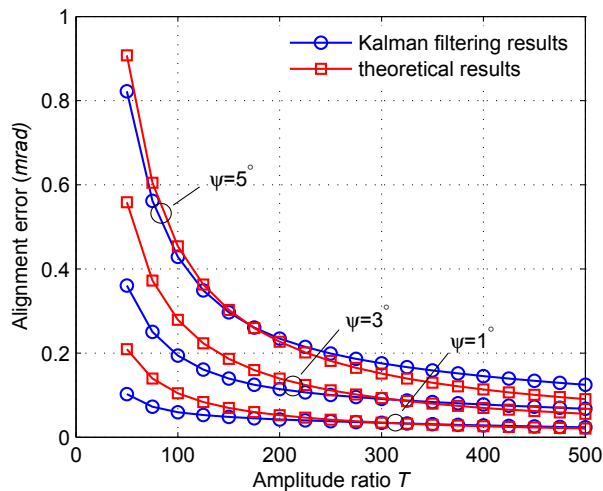
In high-accuracy TA, the course alignment in the TA procedure can accurately estimate the static component ϕ_0 in φ and compensates it. Therefore, φ is very small and equation (61) can further be approximated as

$$\Delta\phi_0 \approx \frac{\psi}{2T}. \quad (62)$$

Equation (62) reveals that the coupling error is proportional to the phase delay angle ψ and is inversely proportional to the amplitude ratio T . Figure 8 plots the approximate coupling error curves of equation (62) as the function of the amplitude ratio $T_x = T_y = T_z = T$ for different values of the phase delay angle $\psi_x = \psi_y = \psi_z = \psi$, labelled as theoretical results, in comparison with the simulated alignment errors obtained by the TA procedure shown in Figure 6, labelled as Kalman filtering results. It can be seen that the theoretical alignment error approximation of equation (62) agrees with the simulated alignment error obtained by the TA procedure.

The above analysis as well as the simulated results of Subsection 4.1 demonstrate that the coupling error is an inherent error source for angular velocity or attitude-based alignment, which depends on the phase delay angle and amplitude ratio of the dynamic flexure and ship angular motion. Ship vibration model analysis shows that the phase delay angle and amplitude transfer ratio are dominated by the ship normal mode, damping ratio and frequency ratio, which may be calculated from ship structure analysis and hydrodynamic analysis. After the phase delay angle and amplitude ratio are determined, the coupling error may be deduced using equation (49).

Figure 8 Comparison of the theoretical alignment error as the function of the amplitude ratio $T_x = T_y = T_z = T$ for different phase delay angle values $\psi_x = \psi_y = \psi_z = \psi$ (see online version for colours)



5 Conclusions

The coupling influence of dynamic flexure with ship angular motion for high accuracy TA has been investigated in this paper. Our motivation to this study has been the observation that the standard transfer alignment procedure may exhibit a large static estimation error even with the high-quality gyro-based MINS and SINS in real shipboard measurements and laboratory experiments. A simplified Bernoulli-Euler beam has been used to obtain the mathematical relationship between the dynamic flexure and the ship angular motion, based on which the gyro data are simulated. Simulation results obtained using the standard TA procedure have shown that the alignment error depends on the phase delay angle as well as the amplitude ratio of the ship dynamic flexure and angular velocity. The theoretical coupling error function has been deduced based on a geometric modelling and mathematical analysis, which shows good agreement with the simulated results obtained by the TA procedure.

The current study points out a potential way of enhancing TA accuracy. If the phase delay angle and amplitude ratio between ship dynamic flexure and angular velocity can be estimated, for example, based on ship structural and hydrodynamic analysis, the coupling error can be estimated. Our future research will investigate a complete solution for compensating this coupling error in order to improve the TA accuracy, for example, by exploiting adaptive control techniques for ship course (Wang et al., 2011).

References

- Abu-Hilal, M. and Mohsen, M. (2000) 'Vibration of beams with general boundary conditions due to a moving random load', *J. Sound and Vibration*, Vol. 232, No. 4, pp.703–717.
- Browne, B.H. and Lackowski, D.H. (1976) 'Estimation of dynamic alignment errors in shipboard firecontrol systems', in *Proc. IEEE Conf. Decision and Control*, Clearwater, USA, December 1–3, pp.48–57.
- Day, D.L. and Arrud, J. (1999) 'Impact of structural flexure on precision tracking', *Naval Engineers Journal*, Vol. 111, No. 3, pp.133–138.
- Groves, P.D. (2003) 'Optimising the transfer alignment of weapon INS', *The Journal of Navigation*, Vol. 56, No. 2, pp.323–335.
- Gu, P., Gundersen, R., Kalvik, A.O., Salvesen, R., Karimi, H.R. and Ottestad, M. (2011) 'Data gathering and mathematical modelling for pitch stabilisation of a high speed catamaran', *Int. J. Modelling, Identification and Control*, Vol. 14, No. 3, pp.149–158.
- Jensen, J.J. and Dogliani, M. (1996) 'Wave-induced ship hull vibrations in stochastic seaways', *Marine Structures*, Vol. 9, Nos. 3–4, pp.353–387.
- Joon, L. and Lim, Y.C. (2009) 'Transfer alignment considering measurement time delay and ship body flexure', *J. Mechanical Science and Technology*, Vol. 23, No. 1, pp.195–203.
- Kain, J.E. and Cloutier, J.R. (1989) 'Rapid transfer alignment for tactical weapon applications', in *Proc. AIAA Conf. Guidance, Navigation and Control*, Boston, USA, August 14–16, pp.1290–1300.
- Lawrence, C.B. (1966) 'Master reference system for rapid at sea alignment of aircraft inertial navigation systems', in *Proc. AIAA/JACC Conf. Guidance and Control*, Seattle, USA, August 15–17, pp.593–606.
- Lee, J. and Whaley, P.W. (1976) 'Prediction of the angular vibration of aircraft structures', *J. Sound and Vibration*, Vol. 49, No. 4, pp.541–549.
- Majeed, S. and Fang, J. (2009) 'Comparison of INS based angular rate matching methods for measuring dynamic deformation', in *Proc. 9th Int. Conf. Electronic Measurement & Instruments*, Beijing, China, August 16–19, pp.332–336.
- Mochalov, A.V. (1999) 'A system for measuring deformations of large-sized objects', in Loukianov, D., Rodloff, R., Sorg, H. and Stieler, B. (Eds.): *Optical Gyros and Their Application* (RTO AGARDograph 339), Canada Communication Group Inc., pp.1–9.
- Mochalov, A.V. and Kazantsev, A.V. (2002) 'Use of the ring laser units for measurement of the moving object deformation', in *Proc. SPIE 4680*, February 5, pp.85–92.
- Petovello, M.G., O'Keefe, K., Lachapelle, G. and Cannon, M.E. (2009) 'Measuring aircraft carrier flexure in support of autonomous aircraft landings', *IEEE Trans. Aerospace and Electronic Systems*, Vol. 45, No. 2, pp.523–535.
- Schnider, A.M. (1983) 'Kalman filter formulations for transfer alignment of strapdown inertial units', *Navigation*, Vol. 30, No. 1, pp.72–89.
- Spalding, K. (1992) 'An efficient rapid transfer alignment filter', in *Proc. AIAA Conf. Guidance, Navigation and Control*, Head Island, USA, August 10–12, pp.1276–1286.
- Sun, F., Guo, C.J., Gao, W. and Li, B. (2007) 'A new inertial measurement method of ship dynamic deformation', in *Proc. Int. Conf. Mechatronics and Automation*, Harbin, China, August 5–8, pp.3407–3412.

Wang, Y., Guo, C., Sun, F., Shen, Z. and Guo, D. (2011) ‘Dynamic neural-fuzzified adaptive control of ship course with parameter modelling uncertainties’, *Int. J. Modelling, Identification and Control*, Vol. 13, No. 4, pp.251–258.

Watanabe, I. and Soares, C.G. (1999) ‘Comparative study on the time-domain analysis of non-linear ship motions and loads’, *Marine Structures*, Vol. 12, No. 3, pp.153–170.

Wu, J.S. and Sheu, J.J. (1996) ‘An exact solution for a simplified model of the heave and pitch motions of a ship hull due to a moving load and a comparison with some experimental results’, *J. Sound and Vibration*, Vol. 192, No. 2, pp.495–520.

Zhang, H-H., Liu, Z-Z., Meng, X-Y. and Li, Y-W. (2012) ‘The D-S theory algorithm with application in the strap-down inertial navigation system’, *Int. J. Modelling, Identification and Control*, Vol. 16, No. 3, pp.259–264.

Zheng, J.X., Qin, S.Q., Wang, X.S. and Huang, Z.S. (2011) ‘Influences of gyro biases on ship angular flexure measurement’, in *Proc. 2011 Symp. Photonics and Optoelectronics*, Wuhan, China, May 16–18, pp.1–4.

Notes

1 The data are classified.

Appendix

Figure 9 shows the spatial relationship between the ship motion direction \vec{r}_m measured by the MINS frame and the motion direction \vec{r}_s measured by the SINS frame, where the Euler angle $\varphi = [\varphi_x \ \varphi_y \ \varphi_z]^T$ denotes the rotation angle from the MINS frame to the SINS frame which consists of a time-invariant component $\phi_0 = [\phi_{0x} \ \phi_{0y} \ \phi_{0z}]^T$ and a time-dependent component $\theta = [\theta_x \ \theta_y \ \theta_z]^T$. As can be seen from Figure 9, the ship motion direction measured by the SINS can be obtained by rotating \vec{r}_m by the angle of φ , and this rotation procedure can be expressed by

$$\vec{r}_s = C(\varphi)\vec{r}_m = C(\theta)C(\phi_0)\vec{r}_m, \tag{63}$$

where $C(\varphi)$ is known as the direction cosine matrix (DCM) of φ , which takes the form

$$C(\varphi) = \begin{bmatrix} \cos \varphi_y \cos \varphi_z & \sin \varphi_x \sin \varphi_y \cos \varphi_z & \cos \varphi_x \sin \varphi_y \cos \varphi_z \\ \cos \varphi_y \sin \varphi_z & \sin \varphi_x \sin \varphi_y \sin \varphi_z & \cos \varphi_x \sin \varphi_y \sin \varphi_z \\ -\sin \varphi_y & \sin \varphi_x \cos \varphi_y & \cos \varphi_x \cos \varphi_y \end{bmatrix}, \tag{64}$$

while the DCMs $C(\phi_0)$ and $C(\theta)$ take the same form of equation (64) by substituting φ with ϕ_0 and θ , respectively. The relationship (63) is equivalent to

$$C(\varphi) = C(\theta)C(\phi_0). \tag{65}$$

Provided that the misalignment angle can be compensated to within several milliradians using the course estimation results, we have $\cos \varphi_i \approx 1$, $\sin \varphi_i \approx \varphi_i$ and $\varphi_i^3 \ll \varphi_i^2 \ll \varphi_i$, where the index i indicates x , y or z coordinate. Therefore, equation (64) can be approximated as

$$C(\varphi) \approx \begin{bmatrix} 1 & -\varphi_z & \varphi_y \\ \varphi_z & 1 & -\varphi_x \\ -\varphi_y & \varphi_x & 1 \end{bmatrix} = I_3 - \hat{\varphi}, \tag{66}$$

in which $\hat{\varphi}$ is a skew-symmetric matrix with the form

$$\hat{\varphi} = \begin{bmatrix} 0 & -\varphi_z & \varphi_y \\ \varphi_z & 0 & -\varphi_x \\ -\varphi_y & \varphi_x & 0 \end{bmatrix}. \tag{67}$$

Similarly, the DCMs $C(\phi_0)$ and $C(\theta)$ can be approximated respectively as

$$C(\phi_0) \approx I_3 - \hat{\phi}_0, \tag{68}$$

$$C(\theta) \approx I_3 - \hat{\theta}, \tag{69}$$

where the skew-symmetric matrices $\hat{\phi}_0$ and $\hat{\theta}$ have the same form with equation (67).

Substituting equations (66), (68) and (69) into equation (65) as well as neglecting second-order components yield

$$\varphi \approx \phi_0 + \theta. \tag{70}$$

Figure 9 The spatial relationship between the ship motion directions measured by the MINS and the SINS

